Surface versus localized plasmons in an assembly of metal-dielectric parallel flat slabs in the presence of an in-plane magnetic field

Yakov M. Strelniker[1,*] and David J. Bergman [2,†]

[1]*Department of Physics, Bar-Ilan University, IL-52900 Ramat-Gan, Israel*
[2]*Raymond and Beverly Sackler School of Physics and Astronomy, Faculty of Exact Sciences,*
Tel Aviv University, IL-69978 Tel Aviv, Israel

Closed-form exact expressions are derived for the macroscopic permittivity tensor of a parallel metal-dielectric sandwichlike composite microstructure in the presence of an externally applied static in-plane magnetic field. An exact closed-form expression for a magnetic-field- and structure-dependent resonance frequency of the multisurface plasmon is obtained. The optical properties of this plasmon are compared with those of the surface plasmons localized around cylindrical holes made in the metallic layers. All analytical results are verified by numerical simulations.

I. INTRODUCTION

The pioneering work of Ebbesen *et al.* [1] on the extraordinary light transmission (ELT) through a periodic array of subwavelength holes in a metal film, or as it is also called, extraordinary optical transmission (a phenomenon that was not discussed in classical diffraction theory [2–4]), led to many publications, experimental as well as theoretical. The ELT effect was explained as being a result of the interaction of light with surface plasmons (SPs). It was assumed that the SPs are localized (or running) on both flat surfaces of the metallic film. However, for simplicity the first publication used the existing theory of SPs excited on a semi-infinite space, as is described, e.g., in the book by Raether [5].

By contrast, in our attempts to understand ELT we considered surface plasmons localized on the surface of circular holes or inclusions but not on the flat film surface [6,7]. It is difficult to distinguish between these two types of plasmons in an experiment since both have the same resonance frequency [$\omega_p/\sqrt{2}$ for running surface plasmons and $\omega_p/\sqrt{n}$ for localized surface plasmons, where $n = 1/2$ is the depolarization factor of a cylinder [6–9], and ω_p is the bulk plasma frequency of the metal constituent; see the sentence right after Eq. (2)]. Only if the holes are not circular but elliptical [8] or when a magnetic field is applied [6–9] will these resonance frequencies differ. The effect of an applied static magnetic field on ELT was discussed in Refs. [6–9]. It was also shown that such a field strongly affects the optical properties of those composites, just as it affects the magnetoresistance properties of such materials (both when the microstructure is periodic [10–14] and when it is disordered [15,16]). The application of a magnetic field converts initially isotropic conductivity and permittivity tensors into anisotropic ones [see Eq. (2)

below]. As a result, the Laplace equation [see Eq. (6) below] for the electric potential also becomes anisotropic. For analytical solving of this problem, it is convenient to perform a coordinate transformation that returns in the virtual space the Laplace equation back to the isotropic form. However, the shape of the inclusions will also be transformed in the virtual space (from spherical or cylindrical to spheroidal or elliptical). Therefore, the depolarization factor $n(\mathbf{H})$ of these figures that are deformed in the virtual space depends on the magnetic field $\mathbf{H}$ and differs from it for the initial spherical (cylindrical) shape of inclusions. As a result, the magnetic field shifts the surface plasmon resonance $\omega_{\mathrm{res}} = \omega_p/\sqrt{n(\mathbf{H})}$ [where $n(\mathbf{H}) \neq 1/2$] and the ELT to higher frequencies. This enables the optical transmissivity of the film to be changed from totally opaque to highly transparent by changing either the magnitude of the magnetic field or its direction [6–12].

In Ref. [17], it was also mentioned that, in addition to surface plasmon resonance, there also exists a so-called cyclotron resonance, which can play, in principle, some role in light transmission. These phenomena can be observed also in Faraday [18], Voigt [18], and Kerr [19,20] rotations as well as in other magneto-optical effects and even in a SPASER [21]. The idea to use the magnetoinduced shift of the surface plasmon frequency in ELT was also discussed later (see, e.g., Refs. [22–31]). It should be mentioned that surface plasmons localized on the surface of spheres in the presence of a magnetic field were already discussed theoretically long ago [32], but not for application to ELT, and not in the framework of the modern metamaterials and plasmonics. The case of running on the surfaces of multislab plasmons also was not considered in Ref. [32]. In a composite medium with a periodic nanostructure, an applied magnetic field can induce a strong anisotropy and make most of the optical properties depend on the direction of the applied magnetic field [6,7]. This is similar to what we recently predicted for the magnetoresistance [10–12,14,15] and thermoelectricity [33,34] in

*strelnik@mail.biu.ac.il
†bergman@tauex.tau.ac.il

such a medium. This was already verified experimentally [35,36] as well as by other theoretical research [37].

Most studies of ELT [38–41] follow Ref. [1] and consider the SP running on the flat surface of a semi-infinite space. From our studies it appears that the situation is more complicated. In particular, if only those resonances are responsible for ELT, then a periodic array of holes in the film would not be required. However, according to Ref. [42], a periodic array of holes or grooves or other (mostly periodic) inhomogeneities or prisms are required in order to excite a SP by interaction with photons. Somewhat later it was observed [43–47] that ELT can appear even when there is only a single aperture in the film. Therefore, the plasmons localized around the hole, which are called localized surface plasmons (LSPs) [5,48,49], should be the cause of ELT. In other experiments it was shown that ELT depends on the shape of the aperture [50,51]. This was explained theoretically in Ref. [8] as resulting from LSPs localized around the apertures. Moreover, in most publications LSPs are mentioned in the case of metallic nanoparticles [52,53] embedded on or near the dielectric surfaces, while on those surfaces there are no (running) SPs. Additional intuitive evidence that it is the LSPs that are important comes from the Keller-Dykhne [54–56] theorem and the Babinet [57] principle.

Following our recent publication devoted to magnetoresistance of flat-slab composites [58], we consider in this paper a metal-dielectric (MD) assembly of parallel flat layers (a sandwichlike geometry that is often used in plasmonic experiments [59–62]). We now find a general analytical asymptotic expression for SPs on the surfaces of the metallic layers that depends on the applied magnetic field, layer permittivities, and their thicknesses. Measurement of the macroscopic permittivity of the sandwich can be used to determine the layer thicknesses, as was pointed out in Ref. [63]. We also find that the discussed resonance can appear only if some special conditions are satisfied. Application of an external static in-plane magnetic field is one way to make such a resonance appear, as we show theoretically. Another way to make this resonance appear, as we show numerically, is by making perforating holes or grooves in the metallic layers. In the latter situation, two types of resonances make an appearance: SPs in a multilayered structure, which is a generalization of the SPs discussed in Refs. [1,5], and the LSP (localized around the holes) as in our previous papers [6,7,17,64,65]. For our theoretical studies we use expressions for the macroscopic dc magnetoresistance of the assembly of parallel layers that were published recently [58] and which we now derive also for the ac case.

The remainder of this article is organized as follows. In Sec. II we develop the theory of magneto-optical properties of an MD assembly of parallel homogeneous and perforated layers in the presence of a static magnetic field. The frequencies of the cyclotron-like and surface-plasmon-like resonances are derived. In particular in Sec. II A we write down expressions for the Drude permittivity and inverse permittivity tensors in the quasistatic approximation. In Sec. II B we derive expressions for the macroscopic effective values of the permittivity tensor. In Sec. II C we find expressions for the resonance frequency of the generalized SP in the presence of a magnetic field. In Sec. II D we derive expressions for the frequencies of the surface plasmon resonances
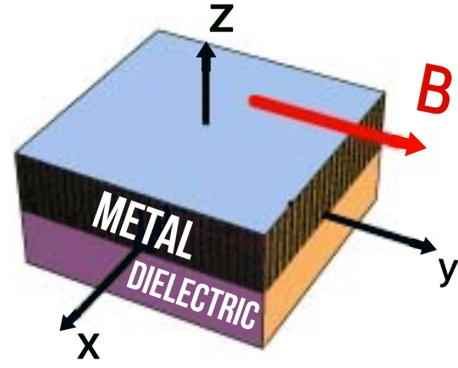

FIG. 1. Schematic representation of the sandwichlike metal-dielectric (MD) assembly of parallel (in the xy-plane and perpendicular to the z-axis) flat slabs. An applied static magnetic field is directed along the y-axis.

in a perforated MD sandwichlike system in the presence of a magnetic field. Our analytical expressions are verified numerically using a numerical approach developed and described in Refs. [6,7,10–12,14,15]. The general solution in this approach is based on a Fourier expansion in the case of composites with a periodic nanostructure. The results of the analytical and numerical calculations are discussed in Sec. III. Section IV provides a summary and discussion of the main results.

II. THEORY

Consider a parallel flat-slabs MD (or semiconductor-dielectric) sandwichlike nanostructure shown schematically in Fig. 1 with x, y-axes of the Cartesian coordinate system parallel and the z-axis perpendicular to the slab planes. An external static magnetic field **B** is applied along the y-axis (see Fig. 1 and the top part of Fig. 2). The local permittivity $\hat{\varepsilon}$ and inverse permittivity $\hat{\eta} \equiv \hat{\varepsilon}^{-1}$ tensors of the conducting and dielectric slabs have the following general forms:

$$\hat{\varepsilon}_i = \begin{pmatrix} \varepsilon_{\perp i} & 0 & \varepsilon_{Hi} \\ 0 & \varepsilon_{\parallel i} & 0 \\ -\varepsilon_{Hi} & 0 & \varepsilon_{\perp i} \end{pmatrix}, \quad \hat{\eta}_i = \begin{pmatrix} \eta_{\perp i} & 0 & \eta_{Hi} \\ 0 & \eta_{\parallel i} & 0 \\ -\eta_{Hi} & 0 & \eta_{\perp i} \end{pmatrix},$$

(1)

where the subscript i equals M when that is the metal constituent and I when that is the dielectric constituent.

A. ac Drude permittivity and inverse permittivity tensors in the quasistatic regime

We will assume everywhere below that the dielectric slabs are characterized by a scalar electrical permittivity $\hat{\varepsilon}_I = \varepsilon_I \hat{\mathbf{I}}$ (where $\hat{\mathbf{I}}$ is the unit tensor), while the conducting slabs are characterized by an ac permittivity tensor $\hat{\varepsilon}_M$. In the presence of a static magnetic field **B** ∥ y (see Fig. 1 and the top part of Fig. 2), $\hat{\varepsilon}_M$ can be written in the Drude approximation as [6,7,18,56,64]

$$\hat{\varepsilon}_M = \varepsilon_0 \hat{\mathbf{I}} + i\frac{4\pi}{\omega}\hat{\sigma} = \varepsilon_0 \hat{\mathbf{I}} + i\omega_p^2 \frac{\tau}{\omega}$$

$$\times \begin{pmatrix} \frac{1-i\omega\tau}{(1-i\omega\tau)^2+H^2} & 0 & \frac{-H}{(1-i\omega\tau)^2+H^2} \\ 0 & \frac{1}{1-i\omega\tau} & 0 \\ \frac{H}{(1-i\omega\tau)^2+H^2} & 0 & \frac{1-i\omega\tau}{(1-i\omega\tau)^2+H^2} \end{pmatrix}.$$
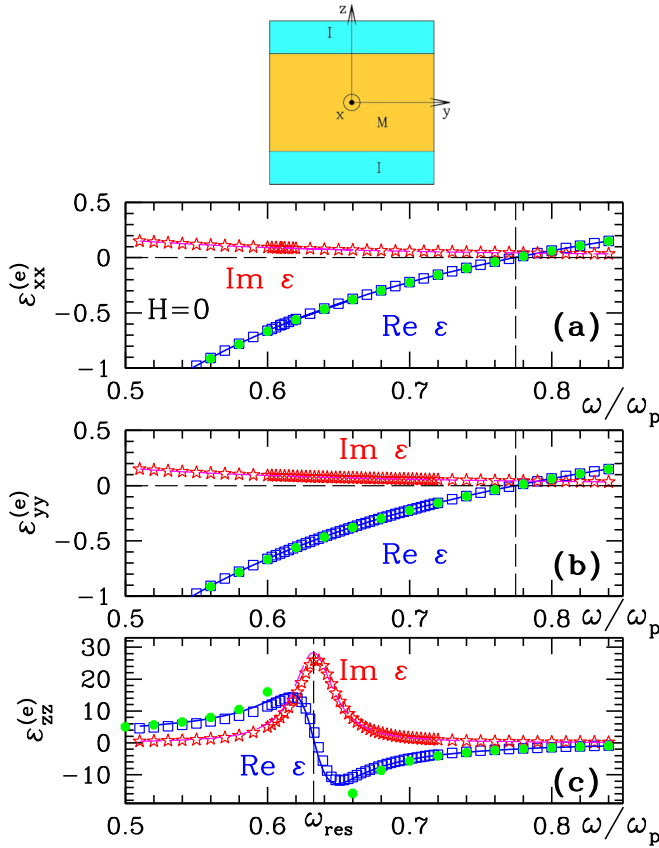
(2)

FIG. 2. (a)–(c) Real (blue) and imaginary (red) parts of the xx, yy, and zz diagonal components of the macroscopic permittivity tensor $\hat{\varepsilon}_e$, of a MD assembly of parallel homogeneous slabs (see Fig. 1 and the top of this figure) vs $\tilde{\omega} \equiv \omega/\omega_p$. $H = 0$. Analytical results [see Eq. (8)] are shown by the solid (for real parts) and dashed (for imaginary parts) lines, while the numerical results are shown by open squares (for real parts) and five pointed open stars (for imaginary parts). In accordance with Eq. (17), the resonance in $\varepsilon_{zz}^{(e)}$ appears at the frequency $\tilde{\omega}_{res} = \sqrt{p_I/\epsilon} = 0.63$ [shown by a vertical dashed line in (c)], while in $\varepsilon_{xx}^{(e)}$ and $\varepsilon_{yy}^{(e)}$ there is no resonance. The vertical dashed line in (a) and (b) shows the frequency $\tilde{\omega} = \sqrt{p_M/\epsilon} = 0.78$ at which $\varepsilon_{xx}^{(e)} = \varepsilon_{yy}^{(e)} = 0$ [see Eq. (21)]. The green dotted lines in (a), (b), and (c) show the asymptotic solutions (21) and (22). Top: Unit cell used for numerical calculations of MD parallel flat-slab nanostructure. Upper and lower "I" slabs are insulating (dielectric) with $\varepsilon_I = 1$ and $p_I = 0.4$, while "M" slab is conducting with $\hat{\varepsilon}_M$ given by Eq. (2) with $\varepsilon_0 = 1$ and $p_M = 0.6$. $\tilde{\tau} = 30$.

Here ε_0 is the scalar dielectric constant of the background ionic lattice, $\omega_p = (4\pi e^2 N_0/m)^{1/2}$ is the plasma frequency,

N_0 is the charge-carrier density, m is the electron mass, $H = |\mathbf{H}| = \omega_c\tau = \mu|\mathbf{B}|$ is the dimensionless form of the magnetic field $\mathbf{B}$, while $\mathbf{B}$ is the magnetic field measured in conventional units, ω_c is the cyclotron frequency, and τ is the conducting relaxation time. When $\omega\tau \gg 1$, Eq. (2) takes the form

$$\hat{\varepsilon}_M = \begin{pmatrix} \varepsilon_0 + \frac{1}{\tilde{H}^2 - \tilde{\omega}^2} & 0 & -\frac{i\tilde{H}}{\tilde{\omega}(\tilde{H}^2 - \tilde{\omega}^2)} \\ 0 & \varepsilon_0 - \frac{1}{\tilde{\omega}^2} & 0 \\ \frac{i\tilde{H}}{\tilde{\omega}(\tilde{H}^2 - \tilde{\omega}^2)} & 0 & \varepsilon_0 + \frac{1}{\tilde{H}^2 - \tilde{\omega}^2} \end{pmatrix}, \quad (3)$$

where we have introduced definitions $\tilde{\omega} \equiv \omega/\omega_p$, $\tilde{\tau} \equiv \tau\omega_p$, and $\tilde{H} \equiv H/\tilde{\tau}$. For $H = 0$, Eq. (3) takes even the simplest form

$$\hat{\varepsilon}_M = \left(\varepsilon_0 - \frac{1}{\tilde{\omega}^2}\right)\hat{\mathbf{I}}, \quad \hat{\eta}_M = \hat{\varepsilon}_M^{-1} = \frac{1}{\varepsilon_0 - \frac{1}{\tilde{\omega}^2}}\hat{\mathbf{I}}. \quad (4)$$

For further treatment, we need the explicit form of the inverse permittivity tensor $\hat{\eta}_M \equiv \varepsilon_M^{-1}$, which follows directly from Eq. (3):

$$\hat{\eta}_M = \varepsilon_M^{-1}$$
$$= \begin{pmatrix} \frac{\varepsilon_0(\tilde{H}^2 - \tilde{\omega}^2) + 1}{\varepsilon_0^2(\tilde{H}^2 - \tilde{\omega}^2) + 2\varepsilon_0 - \frac{1}{\tilde{\omega}^2}} & 0 & \frac{i\tilde{H}}{\tilde{\omega}\left[\varepsilon_0^2(\tilde{H}^2 - \tilde{\omega}^2) + 2\varepsilon_0 - \frac{1}{\tilde{\omega}^2}\right]} \\ 0 & \frac{1}{\varepsilon_0 - \frac{1}{\tilde{\omega}^2}} & 0 \\ \frac{-i\tilde{H}}{\tilde{\omega}\left[\varepsilon_0^2(\tilde{H}^2 - \tilde{\omega}^2) + 2\varepsilon_0 - \frac{1}{\tilde{\omega}^2}\right]} & 0 & \frac{\varepsilon_0(\tilde{H}^2 - \tilde{\omega}^2) + 1}{\varepsilon_0^2(\tilde{H}^2 - \tilde{\omega}^2) + 2\varepsilon_0 - \frac{1}{\tilde{\omega}^2}} \end{pmatrix}. \quad (5)$$

B. Macroscopic effective values of the permittivity tensor

In Ref. [58] we derived exact analytical expressions for the macroscopic resistivity tensor $\hat{\rho}_e$ of a two-constituent flat-slabs composite conductor subjected to an external magnetic field $\mathbf{B}$. In that case, the local potential field $\phi(\mathbf{r})$ obeys the following equation:

$$\nabla \cdot \hat{\sigma}(\mathbf{r}) \cdot \nabla\phi = \mathbf{0}, \quad (6)$$

where $\hat{\sigma}(\mathbf{r}) = \hat{\rho}(\mathbf{r})^{-1}$ is the local conductivity tensor and $\hat{\rho}(\mathbf{r})$ is the local resistivity tensor. Equation (6) is the same as the equation obeyed by $\phi(\mathbf{r})$ in the case under discussion here except that the local resistivity tensor $\hat{\sigma}(\mathbf{r})$ is replaced by the local permittivity tensor $\hat{\varepsilon}(\mathbf{r})$. Because of this, the results for $\hat{\rho}_e$ can immediately be translated into an expression for the macroscopic inverse permittivity tensor $\hat{\eta}_e \equiv \hat{\varepsilon}_e^{-1}$. When the magnetic field $\mathbf{B}$ lies along the y-axis in the slab plane (see Fig. 1) this leads to [see Eqs. (A6)–(A8) in Ref. [58] for $\hat{\rho}_e$]

$$\hat{\eta}_e = \begin{pmatrix} \frac{1}{\frac{p_M}{\eta_{\perp M}} + \frac{p_I}{\eta_{\perp I}}} & 0 & -\frac{p_M\eta_{HM}\eta_{\perp I} + p_I\eta_{HI}\eta_{\perp M}}{p_I\eta_{\perp M} + p_M\eta_{\perp I}} \\ 0 & \frac{1}{\frac{p_M}{\eta_{\parallel M}} + \frac{p_I}{\eta_{\parallel I}}} & 0 \\ \frac{p_M\eta_{HM}\eta_{\perp I} + p_I\eta_{HI}\eta_{\perp M}}{p_I\eta_{\perp M} + p_M\eta_{\perp I}} & 0 & p_M\eta_{\perp M} + p_I\eta_{\perp I} + \frac{(\eta_{HM} - \eta_{HI})^2}{\frac{\eta_{\perp M}}{p_M} + \frac{\eta_{\perp I}}{p_I}} \end{pmatrix}. \quad (7)$$

Here $\eta_{\perp i}$, $\eta_{\parallel i}$, and η_{Hi} $(i = M, I)$ are the transverse, longitudinal (both with respect to magnetic field $\mathbf{B}$), and Hall off-diagonal components of the inverse permittivity tensors of the metal and dielectric constituents, respectively, while p_M and p_I are their volume fractions.

An expression for the macroscopic permittivity tensor $\hat{\varepsilon}_e \equiv \hat{\eta}_e^{-1}$ follows directly from Eq. (7):

$$\hat{\varepsilon}_e = \begin{pmatrix} \dfrac{\left(\frac{p_M}{\eta_{\perp M}} + \frac{p_I}{\eta_{\perp I}}\right)\left(p_M \eta_{\perp M} + p_I \eta_{\perp I} + \frac{\eta_{HM}^2}{\frac{\eta_{\perp M}}{p_M} + \frac{\eta_{\perp I}}{p_I}}\right)}{p_M \eta_{\perp M} + p_I \eta_{\perp I} + \frac{\eta_{HM}^2 p_M}{\eta_{\perp M}}} & 0 & \dfrac{p_M \eta_{HM}}{\eta_{\perp M}\left(p_M \eta_{\perp M} + p_I \eta_{\perp I} + \frac{p_M \eta_{HM}^2}{\eta_{\perp M}}\right)} \\[4mm] 0 & \dfrac{p_M}{\eta_{\parallel M}} + \dfrac{p_I}{\eta_{\parallel I}} & 0 \\[4mm] -\dfrac{p_M \eta_{HM}}{\eta_{\perp M}\left(p_M \eta_{\perp M} + p_I \eta_{\perp I} + \frac{p_M \eta_{HM}^2}{\eta_{\perp M}}\right)} & 0 & \dfrac{1}{p_M \eta_{\perp M} + p_I \eta_{\perp I} + \frac{p_M \eta_{HM}^2}{\eta_{\perp M}}} \end{pmatrix}. \tag{8}$$

In the preceding equation and everywhere below, we have assumed that the Hall tensor component of the dielectric vanishes: $\eta_{HI} = 0$. For $H = 0$ (when $\eta_{\perp i} = 1/\varepsilon_{\perp i}$ and similarly for the longitudinal component of both constituents, $i = I, M$), Eq. (8) simplifies to the following diagonal form:

$$\hat{\varepsilon}_{xx}^{(e)} = \frac{p_M}{\eta_{\perp M}} + \frac{p_I}{\eta_{\perp I}} = p_M \varepsilon_{\perp M} + p_I \varepsilon_{\perp I}, \tag{9}$$

$$\hat{\varepsilon}_{yy}^{(e)} = \frac{p_M}{\eta_{\parallel M}} + \frac{p_I}{\eta_{\parallel I}} = p_M \varepsilon_{\parallel M} + p_I \varepsilon_{\parallel I}, \tag{10}$$

$$\frac{1}{\hat{\varepsilon}_{zz}^{(e)}} = p_M \eta_{\perp M} + p_I \eta_{\perp I} = \frac{p_M}{\varepsilon_{\perp M}} + \frac{p_I}{\varepsilon_{\perp I}}. \tag{11}$$

These are the well-known expressions for the macroscopic effective permittivities of a system of parallel slabs when $H = 0$ (see, e.g., Refs. [66,67]).

C. Resonances

Besides the yy component, all the nonzero tensor components in Eq. (8) have the same denominator. When that denominator vanishes, that signifies a resonance. However, in the case of the xx-component when $H = 0$ the numerator vanishes together with the denominator. Therefore, a resonance appears only when $H \neq 0$. By contrast, the zz-component exhibits a resonance even when $H = 0$.

To find an analytical expression for the resonance frequency and its dependence on the magnetic field H, it is enough to substitute Eq. (5) into Eq. (8). We thus get the following expression for the macroscopic tensor $\hat{\varepsilon}_e$:

$$\hat{\varepsilon}_e = \begin{pmatrix} \dfrac{\bar{\varepsilon}}{\tilde{\omega}^2}\dfrac{P_4(\tilde{\omega})}{P_3(\tilde{\omega})} & 0 & -\dfrac{i\varepsilon_I}{\epsilon\tilde{\omega}}\dfrac{p_M \tilde{H}}{\tilde{\omega}^2 - \left(\frac{p_I}{\epsilon} + \tilde{H}^2\right)} \\[3mm] 0 & \bar{\varepsilon} - \dfrac{p_M}{\tilde{\omega}^2} & 0 \\[3mm] \dfrac{i\varepsilon_I}{\epsilon\tilde{\omega}}\dfrac{p_M \tilde{H}}{\tilde{\omega}^2 - \left(\frac{p_I}{\epsilon} + \tilde{H}^2\right)} & 0 & -\dfrac{\varepsilon_I}{\epsilon}\dfrac{\varepsilon_0(\tilde{H}^2 - \tilde{\omega}^2) + 1}{\tilde{\omega}^2 - \left(\frac{p_I}{\epsilon} + \tilde{H}^2\right)} \end{pmatrix}, \tag{12}$$

where we have introduced the weighted arithmetic permittivity $\bar{\varepsilon}$ and a combination ϵ of permittivities, respectively:

$$\bar{\varepsilon} \equiv p_M \varepsilon_0 + p_I \varepsilon_I, \tag{13}$$

$$\epsilon \equiv p_M \varepsilon_I + p_I \varepsilon_0 = \varepsilon_I \varepsilon_0 \left(\frac{p_M}{\varepsilon_0} + \frac{p_I}{\varepsilon_I}\right). \tag{14}$$

$P_3(\tilde{\omega})$ in the denominator of $\hat{\varepsilon}_{xx}^{(e)}$ [see Eq. (12)] is a polynomial of the third degree in $\tilde{\omega}^2$, which, after regrouping of its terms and after some algebra, can be expressed as

$$P_3(\tilde{\omega}) = \tilde{\omega}^6 - \left[2\left(\tilde{H}^2 + \frac{1}{\varepsilon_0}\right) + \frac{p_I}{\epsilon}\right]\tilde{\omega}^4 + \left[\left(\tilde{H}^2 + \frac{1}{\varepsilon_0}\right)^2 + \frac{p_I}{\epsilon}\left(\tilde{H}^2 + \frac{2}{\varepsilon_0}\right)\right]\tilde{\omega}^2 - \frac{1}{\varepsilon_0^2}\left(\tilde{H}^2 + \frac{p_I}{\epsilon}\right)$$

$$= \left[\tilde{\omega}^2 - \left(\frac{p_I}{\epsilon} + \tilde{H}^2\right)\right]\left[\tilde{\omega}^4 - \left(\tilde{H}^2 + \frac{2}{\varepsilon_0}\right)\tilde{\omega}^2 + \frac{1}{\varepsilon_0^2}\right] = \left[\tilde{\omega}^2 - \left(\frac{p_I}{\epsilon} + \tilde{H}^2\right)\right](\tilde{\omega}^2 - \omega_1^2)(\tilde{\omega}^2 - \omega_2^2). \tag{15}$$

In these equations, we have introduced the following quantities:

$$\omega_{1,2}^2 \equiv \frac{2 + \varepsilon_0 \tilde{H}^2 \pm \varepsilon_0^{1/2}\tilde{H}\sqrt{4 + \varepsilon_0 \tilde{H}^2}}{2\varepsilon_0}. \tag{16}$$

The first set of parentheses on the right-hand side of Eq. (15) determines a general expression for the resonance frequency $\tilde{\omega}_{\text{res}}$ of the surface plasmon, which depends on the permittivities ε_I, ε_0 of the slabs, their thicknesses, and the applied magnetic field:

$$\widetilde{\omega}_{\text{res}} \equiv \frac{\omega_{\text{res}}}{\omega_p} = \sqrt{\frac{p_I}{\epsilon} + \tilde{H}^2} = \sqrt{\frac{p_I}{p_M \varepsilon_I + p_I \varepsilon_0} + \left(\frac{\omega_c}{\omega_p}\right)^2}. \tag{17}$$

When $H = 0$ and $p_I = p_M = 1/2$, this expression reduces to the resonance frequency of Eq. (2.8) in Ref. [5] (the correct expression for that quantity, which is discussed later in many publications related to ELT [1], would be $\omega_{\text{res}} = \omega_p/\sqrt{\varepsilon_0 + \varepsilon_I}$).

When $H \neq 0$ but still $p_I = p_M = 1/2$, Eq. (17) is similar (with precision up to a factor before ω_c) to Eq. (5) in Ref. [68] (see also Refs. [69,70]). When $p_I = 0$, i.e., in an infinite homogeneous conductor, ω_{res} reduces to the cyclotron resonance ω_c [see Eq. (3) above and Refs. [17,71]]. The other two sets of parentheses on the right-hand side of Eq. (15) also pass through zero, but they do not contain any information about the system microstructure. Therefore they cannot be resonances, and the only possibility is that they should cancel with the numerator. Using this observation, we express the polynomial $P_4(\tilde{\omega})$ in the numerator of $\hat{\varepsilon}_{xx}^{(e)}$, which is of the fourth degree in $\tilde{\omega}^2$, as

$$P_4(\tilde{\omega}) = \tilde{\omega}^8 - \left[2\left(\tilde{H}^2 + \frac{1}{\varepsilon_0}\right) + \frac{p_M}{\bar{\varepsilon}} + \frac{p_I}{\epsilon} \right]\tilde{\omega}^6 + \left[\left(\tilde{H}^2 + \frac{1}{\varepsilon_0}\right)^2 + \left(\tilde{H}^2 + \frac{2}{\varepsilon_0}\right)\left(\frac{p_M}{\bar{\varepsilon}} + \frac{p_I}{\epsilon}\right) + \frac{p_M}{\bar{\varepsilon}}\frac{p_I}{\epsilon} \right]\tilde{\omega}^4$$

$$- \left[\frac{1}{\varepsilon_0}\left(\tilde{H}^2 + \frac{1}{\varepsilon_0}\right)\left(\frac{p_M}{\bar{\varepsilon}} + \frac{p_I}{\epsilon}\right) + \frac{p_M}{\bar{\varepsilon}}\frac{p_I}{\epsilon}\left(\frac{2}{\varepsilon_0} + \frac{\varepsilon_I^2}{\varepsilon_0^2}\tilde{H}^2\right) \right]\tilde{\omega}^2 + \frac{1}{\varepsilon_0^2}\frac{p_M}{\bar{\varepsilon}}\frac{p_I}{\epsilon} \tag{18}$$

$$= \left[\tilde{\omega}^4 - \left(\tilde{H}^2 + \frac{2}{\varepsilon_0}\right)\tilde{\omega}^2 + \frac{1}{\varepsilon_0^2} \right]\left[\tilde{\omega}^4 - \left(\frac{p_M}{\bar{\varepsilon}} + \frac{p_I}{\epsilon} + \tilde{H}^2\right)\tilde{\omega}^2 + \frac{p_I}{\epsilon}\frac{p_M}{\bar{\varepsilon}} \right]. \tag{19}$$

Here we have taken into account that $\epsilon\bar{\varepsilon} = \varepsilon_I\varepsilon_0 + p_I p_M(\varepsilon_I - \varepsilon_0)^2$, $p_M\epsilon + p_I\bar{\varepsilon} = \varepsilon_I + 2p_M p_I(\varepsilon_0 - \varepsilon_I)$, and $p_I^2 + p_M^2 + 2p_I p_M = 1$, as follows from Eqs. (13) and (14). Finally, Eq. (12) simplifies to

$$\hat{\varepsilon}_e = \begin{pmatrix} \dfrac{\bar{\varepsilon}}{\tilde{\omega}^2}\dfrac{\tilde{\omega}^4 - \left(\frac{p_M}{\bar{\varepsilon}} + \frac{p_I}{\epsilon} + \tilde{H}^2\right)\tilde{\omega}^2 + \frac{p_I}{\epsilon}\frac{p_M}{\bar{\varepsilon}}}{\tilde{\omega}^2 - \left(\frac{p_I}{\epsilon} + \tilde{H}^2\right)} & 0 & -\dfrac{i\varepsilon_I}{\epsilon\tilde{\omega}}\dfrac{p_M\tilde{H}}{\tilde{\omega}^2 - \left(\frac{p_I}{\epsilon} + \tilde{H}^2\right)} \\ 0 & \bar{\varepsilon} - \dfrac{p_M}{\tilde{\omega}^2} & 0 \\ \dfrac{i\varepsilon_I}{\epsilon\tilde{\omega}}\dfrac{p_M\tilde{H}}{\tilde{\omega}^2 - \left(\frac{p_I}{\epsilon} + \tilde{H}^2\right)} & 0 & -\dfrac{\varepsilon_I}{\epsilon}\dfrac{\varepsilon_0(\tilde{H}^2 - \tilde{\omega}^2) + 1}{\tilde{\omega}^2 - \left(\frac{p_I}{\epsilon} + \tilde{H}^2\right)} \end{pmatrix}. \tag{20}$$

It follows from Eq. (8) that, when $H = 0$, the bracket with resonance (17) should disappear in the xx tensor component but should remain in the zz component (see Figs. 2 and 3). At $H = 0$, the numerator of the xx component of the tensor $\hat{\varepsilon}_e$ in Eq. (20) can be expressed in the form $(\tilde{\omega}^2 - \frac{p_I}{\epsilon})(\tilde{\omega}^2 - \frac{p_M}{\bar{\varepsilon}})$. Therefore, the term $(\tilde{\omega}^2 - \frac{p_I}{\epsilon})$ cancels out in the denominator and the numerator. Finally, when $H = 0$ the nonzero

FIG. 3. The same as Fig. 2 but for $\varepsilon_I = 3$. The resonance in $\varepsilon_{zz}^{(e)}$ appears at the frequency $\tilde{\omega}_{\mathrm{res}} = \sqrt{p_I/\epsilon} = 0.43$ [see Eq. (17)] shown in (c) by a vertical dashed line, while in $\varepsilon_{xx}^{(e)}$ and $\varepsilon_{yy}^{(e)}$ there is no resonance. The green dotted curves in (a), (b), and (c) show the asymptotic solutions (21) and (22). The vertical dashed lines in (a) and (b) show the frequency $\tilde{\omega} = \sqrt{p_M/\bar{\varepsilon}}$ at which $\varepsilon_{xx}^{(e)} = \varepsilon_{yy}^{(e)} = 0$ [see Eq. (21)].

components of the tensor (20) become

$$\varepsilon_{xx}^{(e)} = \varepsilon_{yy}^{(e)} = \bar{\varepsilon} - \frac{p_M}{\tilde{\omega}^2}, \tag{21}$$

$$\varepsilon_{zz}^{(e)} = -\frac{\varepsilon_I}{\epsilon}\frac{1 - \varepsilon_0\tilde{\omega}^2}{\tilde{\omega}^2 - \frac{p_I}{\epsilon}} = \frac{\varepsilon_I(\varepsilon_0\tilde{\omega}^2 - 1)}{\epsilon\tilde{\omega}^2 - p_I}. \tag{22}$$

From Eq. (22) and Figs. 2 and 3 it is evident that the resonance in the $\varepsilon_{zz}^{(e)}$ component exists even when $H = 0$. Therefore, ELT should appear in the absence of a magnetic field when the light beam is incident on the sample parallel to the slabs and is polarized along the z axis (see Fig. 1). By contrast, the resonance in the yy tensor component will never be observed, either with or without an applied magnetic field. This differs from LSP, which exhibits the resonance in both the transverse and the longitudinal tensor components—see below.

When $\varepsilon_0 = 1$ and $\varepsilon_I = 1$, Eq. (20) for arbitrary H simplifies to

$$\hat{\varepsilon}_e = \begin{pmatrix} \dfrac{1}{\tilde{\omega}^2}\dfrac{(\tilde{\omega}^2 - \omega_3^2)(\tilde{\omega}^2 - \omega_4^2)}{\tilde{\omega}^2 - (p_I + \tilde{H}^2)} & 0 & \dfrac{i}{\tilde{\omega}}\dfrac{p_M\tilde{H}}{\tilde{\omega}^2 - (p_I + \tilde{H}^2)} \\ 0 & 1 - \dfrac{p_M}{\tilde{\omega}^2} & 0 \\ -\dfrac{i}{\tilde{\omega}}\dfrac{p_M\tilde{H}}{\tilde{\omega}^2 - (p_I + \tilde{H}^2)} & 0 & -\dfrac{1 - \tilde{\omega}^2 + \tilde{H}^2}{\tilde{\omega}^2 - (p_I + \tilde{H}^2)} \end{pmatrix}, \tag{23}$$

where

$$\omega_{3,4}^2 = \frac{1}{2}\left(1 + \tilde{H}^2 \pm \sqrt{(\tilde{H}^2 + 1)^2 - 4p_M p_I}\right). \tag{24}$$

We now discuss the behavior of the xx component of $\hat{\varepsilon}_e$. When this was done by using reductions in the numerator and denominator, the results were very instructive: When each layer is homogeneous, the x and y directions are equivalent and the vanishing of the denominator of $\varepsilon_{xx}^{(e)}$ is canceled by the coincident vanishing of the numerator. This symmetry of $\hat{\varepsilon}_e$ is spoiled when an external magnetic field is present. This leads to the appearance of a resonance in $\varepsilon_{xx}^{(e)}$. As we already pointed out earlier, it follows from Eq. (8) that when $H = 0$,
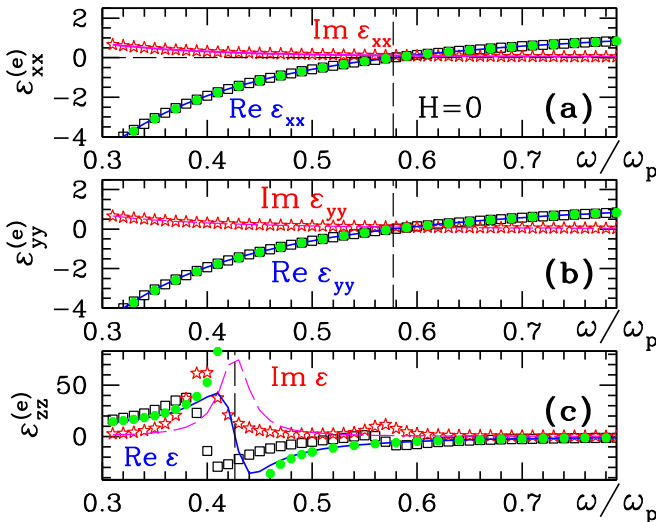
there should not be any resonance in the xx tensor component. However, in many experiments there are small nonzero values of H. We also speculate that the exact cancellation of the vanishing numerator and denominator is not a stable situation and that any structural perturbation of the uniform flat layers can spoil this, not only the presence of a small magnetic field. For example, the rotational symmetry of the microstructure in the x, y-plane is spoiled when the layer includes holes or grooves. Below we will show numerically that holes in the metallic layers, or grooves on the top and bottom of such a layer, or other deformations of these layers, can change the expressions of the numerator and denominator in such a way that the coincident vanishing will not occur anymore (see Figs. 10–12). This is qualitatively similar to what was observed and discussed in the case of ELT [1,38,72], where in order to excite the SP one needed to have a periodic array of holes or grooves or to attach glass prisms [1].

From Eq. (17) it follows that application of a magnetic field $\mathbf{B} \parallel y$ (see Fig. 1) induces the plasmonlike resonance of Eq. (17). It is natural to expect that this resonance will lead to ELT phenomena, i.e., transparency. In fact, if we assume that light is polarized along the x axis, then the refractive index should be equal to $n_x = \sqrt{\varepsilon_{xx}^{(e)}}$. Using, for simplicity, the formula for light reflection, R, and transmission, T, coefficients, derived for the case of a semi-infinite space: $R = |(n_x - 1)/(n_x + 1)|^2$ (where $n_x = \sqrt{\varepsilon_{xx}^{(e)}}$) and $T = 1 - R$, we obtain ELT transmission, as evident in Figs. 8(a) and 8(b). However, in the presence of a magnetic field, light is in fact elliptically polarized [18] with a refractive index $n_\perp^2 = \varepsilon_{xx}^{(e)} + \frac{|\varepsilon_{xz}^{(e)}|^2}{\varepsilon_{zz}^{(e)}}$. From Eq. (8) it follows directly that the latter expression has no resonance:

$$n_\perp^2 = \varepsilon_{xx}^{(e)} + \frac{\left|\varepsilon_{xz}^{(e)}\right|^2}{\varepsilon_{zz}^{(e)}} = \frac{p_M}{\eta_{\perp M}} + \frac{p_I}{\eta_{\perp I}}, \qquad (25)$$

which is qualitatively similar to the expression for $n_\parallel^2 = \varepsilon_{yy}^{(e)}$. Substituting Eq. (5) into Eq. (25), it follows that $n_\perp^2 = 1 + \frac{p_M(1 - 1/\tilde{\omega}^2)}{1 - (\tilde{H}^2 - \tilde{\omega}^2)}$. Therefore, there is no nanostructure-dependent resonance in $n_\perp$, and ELT cannot be observed [see Fig. 8(c)].

D. Surface plasmons localized around circular holes: Numerical scheme for periodic composite, dilute, and Clausius-Mossotti approximations

The theory described in Secs. II B and II C was developed for the case of homogeneous slabs. To account for holes, grooves, and other inhomogeneities, one needs to complement it by other approaches, such as the effective-medium approximation (EMA) or numerical calculations.

1. Numerical scheme for a composite with periodic nanostructures

In the case of a periodic array of holes or grooves, we can use our numerical scheme developed for calculations of magnetoresistance, magneto-optical, and thermoelectric effects in periodic composites and in the presence of the magnetic field. We treat the holes as dielectric inclusions with permittivity $\hat{\varepsilon}_I$ embedded in a conducting host with permittivity tensor $\hat{\varepsilon}_M$ given by Eq. (2), while the entire position-dependent permittivity tensor can be written as $\hat{\varepsilon}(r) = \hat{\varepsilon}_I \theta_1(\mathbf{r}) + \hat{\varepsilon}_M \theta_2(\mathbf{r})$. Here

$\theta_1(\mathbf{r})$ is the characteristic function describing the location and the shape of the inclusions ($\theta_1 = 1$ inside the inclusions and $\theta_1 = 0$ outside of them), while θ_2 is a similar characteristic function describing the location and the shape of the host $\theta_2 = 1 - \theta_1$. Then Eq. (6) can be rewritten as

$$\nabla \cdot \hat{\varepsilon}(\mathbf{r}) \cdot \nabla \phi^{(\alpha)} = \nabla \cdot \theta_1 \hat{\delta \varepsilon} \cdot \nabla \phi^{(\alpha)}, \qquad (26)$$

where $\delta \hat{\varepsilon} \equiv \hat{\varepsilon}_2 - \hat{\varepsilon}_1$. Following Refs. [6–12,14,15,17,18,33,34], we chose a scheme where the composite medium occupies the entire volume between the infinitely conducting plates of a large parallel plate capacitor. In this approach, the local electric potential $\phi(\mathbf{r})$ is then the solution of a boundary-value problem based upon the Laplace partial differential equation (26) and the boundary condition $\phi^{(\alpha)} = r_\alpha$. Here r_α is the α-component of the applied voltage $\mathbf{r}$.

When the inclusions are arranged on a three- (3D) or two- (2D) dimensional periodic lattice, a more suitable approach is a Fourier expansion technique [7,8,10,11,18]. Since $\theta_1(\mathbf{r})$ and $\psi^{(\alpha)} = \phi^{(\alpha)} - r^{(\alpha)}$ are now periodic functions, they can be expanded in a Fourier series. This transforms Eq. (26) into an infinite set of linear algebraic equations for the Fourier coefficients,

$$\psi_\mathbf{g} = \frac{1}{V} \int_V \psi^{(\alpha)}(\mathbf{r}) e^{-i\mathbf{g} \cdot \mathbf{r}} dV, \qquad (27)$$

where $\mathbf{g} = (2\pi/d)(m_x, m_y, m_z)$ is a vector of the appropriate reciprocal lattice, m_i are arbitrary integers, d is a lattice constant, and V is the volume of a unit cell. After solving a truncated, finite subset of those linear algebraic equations [6–12,14,15,17,18,33,34] resulting from Eq. (26), we can use those Fourier coefficients $\psi_\mathbf{g}^{(\alpha)}$ in order to calculate the bulk effective macroscopic electric permittivity tensor $\hat{\varepsilon}_e$, using the procedure described in Refs. [7,8,10,11,18]. The analytical expressions for the Fourier coefficient $\theta_\mathbf{g}$ of the $\theta_1(\mathbf{r})$ function for different shapes of inclusions are given in Refs. [7–11,18].

The accuracy of this numerical approach depends on the number of components included in the Fourier expansion. That number used in our 3D calculations was between 20 and 28 components in each direction, which resulted in a very time-consuming computation even for a supercomputer. In some cases, the 3D problem could be reduced to a 2D problem and then we used up to 90 Fourier components in each direction. The results of such numerical calculations are shown in Figs. 10–12.

2. Dilute and Clausius-Mossotti approximations

The resonance frequency that is due to the presence of a cylindrical hole in the middle of each unit cell (see the top part of Fig. 10) can be calculated, e.g., by assuming a *dilute* collection of parallel right-circular cylindrical inclusions inside a metal host. Then the method of dilute approximation (DA) can be applied. This approximation does not take into account the periodicity of the microstructure. The ii component of the permittivity tensor in this approximation has the form [7,8,64,65,73]

$$\varepsilon_{ii}^{(e)} = \varepsilon_{M\,ii} \left[1 - p_{\text{cyl}} \frac{\delta \varepsilon_{ii}}{\varepsilon_{M\,ii} - \mathsf{n}_i(H) \delta \varepsilon_{ii}} \right], \qquad (28)$$

where p_{cyl} is the volume fraction of the cylindrical inclusions, $\delta \varepsilon_{ii} = \varepsilon_{M\,ii} - \varepsilon_{I\,ii}$, and $\mathsf{n}_i(H)$ is the
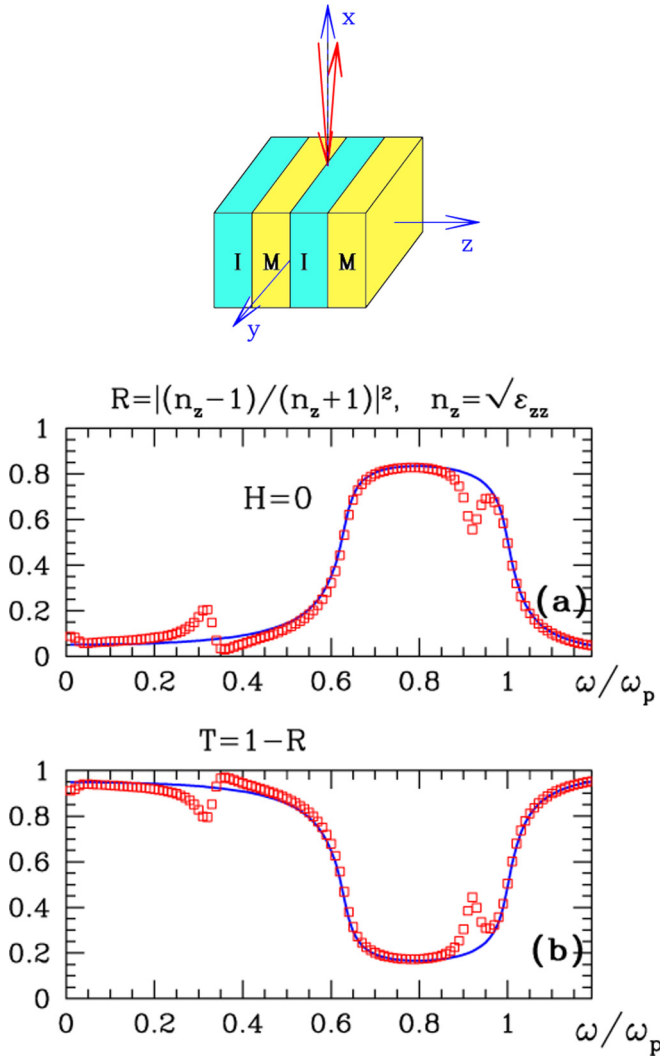
FIG. 4. Reflectance $R = |(n_z - 1)/(n_z + 1)|^2$ (a) and transmittance $T = 1 - R$ (b) vs $\tilde{\omega}$, where the refractive index $n_z = \sqrt{\varepsilon_{zz}^{(e)}}$ is taken from Fig. 2. Analytical results are shown by the solid lines, while the numerical results are shown by open squares.

magnetic-field-dependent depolarization factor [7] along the i-axis. When $i = x$, the depolarization factor is [7] $\mathsf{n}_x(H) = 1/[1 + \sqrt{\varepsilon_{Myy}(H)/\varepsilon_{Mxx}(H)}]$. The spectral dependence of $\varepsilon_{xx}^{(e)}$ on $\tilde{\omega}$ obtained by DA for the different values of H is shown in Fig. 14. Using Eqs. (3) and (28), the resonance frequency $\tilde{\omega}_{\text{res}}$ in the xx tensor component is found to be

$$\tilde{\omega}_{\text{res}} = \sqrt{\frac{1 - \mathsf{n}_x(H)}{\varepsilon_0 - \mathsf{n}_x(H)(\varepsilon_0 - \varepsilon_I)} + \tilde{H}^2}, \quad \text{where } \tilde{H} \equiv \frac{H}{\tilde{\tau}}. \quad (29)$$

When H is small, $\mathsf{n}_x \simeq 1/2$, and $\varepsilon_I = \varepsilon_0 = 1$, then $\tilde{\omega}_{\text{res}} \simeq \sqrt{1/2 + \tilde{H}^2}$ [see Eq. (14)]. For larger values of $\tilde{H}$ the resonance frequency $\tilde{\omega}_{\text{res}}$ can be found numerically from Eq. (15) in Ref. [7]. However, when $\varepsilon_I = \varepsilon_0 = 1$, Eq. (3) leads to the following simple expression:

$$\tilde{\omega}_{\text{res}} = \sqrt{(1 + \tilde{H}^2)/2}. \quad (30)$$
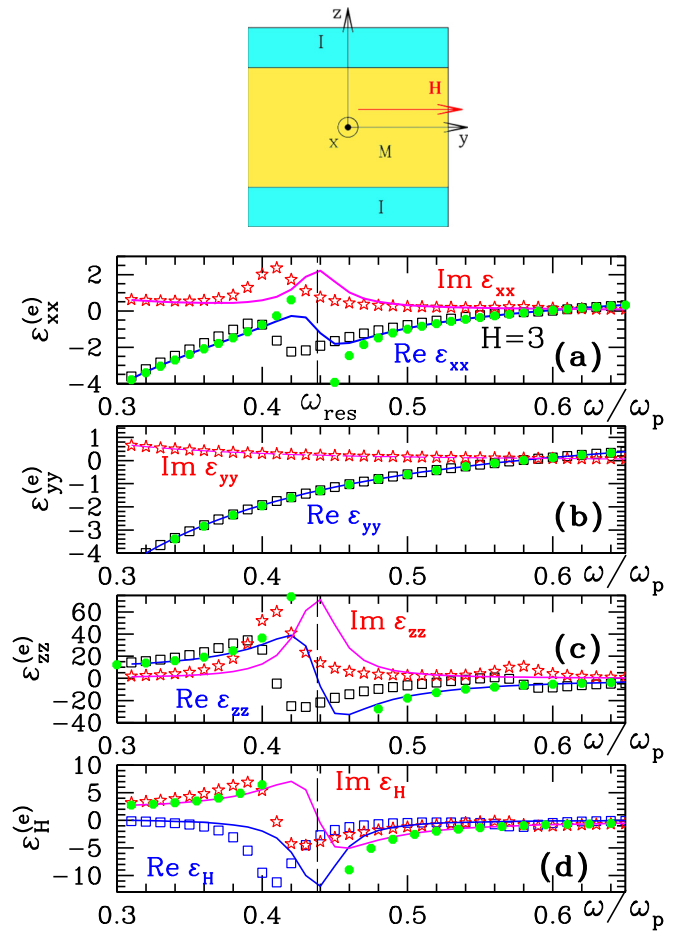

FIG. 5. Similar to Fig. 3 but for $H = 3$ ($\mathbf{H} \parallel y$); see the top part of this figure. In (d) is shown the off-diagonal Hall component $\varepsilon_H^{(e)}$. The resonance appears in $\varepsilon_{xx}^{(e)}$, $\varepsilon_{zz}^{(e)}$, $\varepsilon_H^{(e)}$ at $\tilde{\omega}_{\text{res}} = 0.44$ [see Eq. (17)] shown by a vertical dashed line. The green dotted curves in (a), (b), (c), and (d) show the asymptotic solutions (20).

The value of the resonance $\tilde{\omega}_{\text{res}}$ given by Eq. (28) is correct in the limit where the volume fraction of the cylindrical inclusions is small, i.e., when $p_{\text{cyl}} \ll 1$. In the Clausius-Mossotti (CM) approximation [64,65], Eq. (29) can be corrected by replacing the depolarization factor n_i by the product

$$\mathsf{n}_i \rightarrow (1 - p_{\text{cyl}})\mathsf{n}_i. \quad (31)$$

In that case, and when $\varepsilon_I = \varepsilon_0 = 1$, Eq. (30) transforms to

$$\tilde{\omega}_{\text{res}} = \sqrt{\frac{1 + \tilde{H}^2}{2 - p_{\text{cyl}}}}. \quad (32)$$

E. Reduction of the 3D problem to a 2D problem

As the microstructure under consideration becomes more complicated, more Fourier components are required in order to get good results. A 3D numerical calculation of a system with conducting layers of finite thickness and with fully penetrating holes or non-fully-penetrating grooves on both surfaces is therefore a very time-consuming procedure (see Figs. 10–13 where up to 28 Fourier components were used in all directions). However, we found that it is possible to
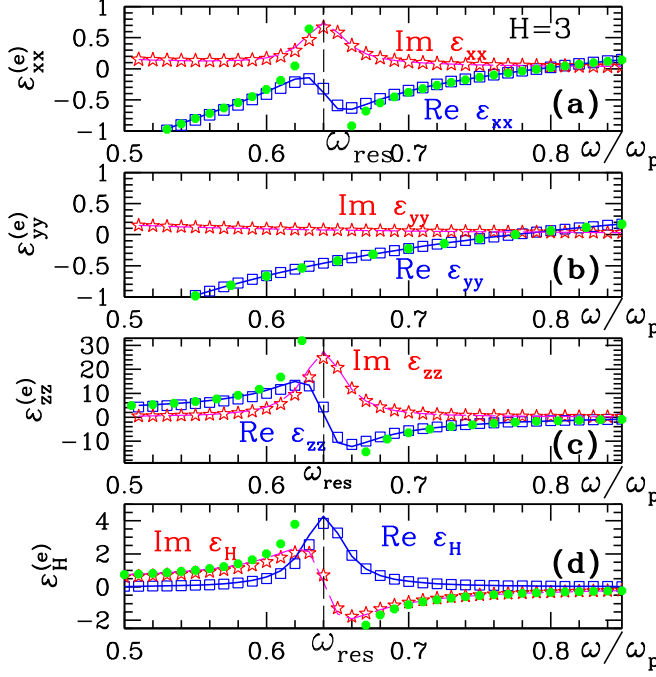
FIG. 6. (a)–(c) Similar to Fig. 5 but with parameters as in Fig. 2 ($p_M = 0.6$, $p_I = 0.4$, $\tilde{\tau} = 30$, $\varepsilon_0 = 1$, $\varepsilon_I = 1$) and $H = 3$. (d) The off-diagonal permittivity tensor component $\varepsilon_H^{(e)} \equiv \varepsilon_{xz}^{(e)}$ vs $\tilde{\omega}$. The green dotted lines show analytical asymptotic results (23). The components $\varepsilon_{xx}^{(e)}$, $\varepsilon_{zz}^{(e)}$, and $\varepsilon_H^{(e)}$ have resonances at $\tilde{\omega}_{res} = \sqrt{p_I/\epsilon + \tilde{H}^2} = 0.64$, while $\varepsilon_{yy}^{(e)}$ has no resonance.

III. RESULTS

reduce the 3D calculation to a 2D calculation. To achieve this, we need to use Eq. (7) or Eq. (8) in which the inverse permittivity tensors of the metal constituent ($\eta_{\perp M}$, $\eta_{\parallel M}$, and $\eta_{H M}$) are replaced by 2D volume-averaged values ($\eta_{\perp M}^{(2De)}$, $\eta_{\parallel M}^{(2De)}$, and $\eta_{H M}^{(2De)}$). That is, we first solve the system of a metal host with a 2D periodic array of infinitely long cylindrical holes, which is in fact a 2D microstructure and therefore needs much fewer Fourier components in the calculation. Then we substitute the values $\eta_M^{(2De)}$ and $\eta_H^{(2De)}$ into Eq. (7) or Eq. (8). In this way, the 3D problem with a complicated microstructure has been transformed into a 2D problem in a microstructure of parallel homogeneous layers. The results of this approach are shown in Figs. 11 and 13 in comparison with direct 3D calculations. This approach is correct only when the condition for homogenization of the metallic slabs is valid, i.e., in the quasistatic approximation when the light wavelength λ is much larger than the radius r of the cylindrical hole and the lattice constant.

III. RESULTS

We have studied the properties of the macroscopic electric permittivity tensor $\hat{\varepsilon}_e$ of a metal (or semiconductor) -dielectric sandwichlike system of parallel slabs (see Fig. 1). For this we use the exact analytical expressions for the dc macroscopic resistivity tensor $\hat{\rho}_e$ recently derived by us in Ref. [58], which we have now rewritten for the ac case. Exact asymptotic expressions for the macroscopic permittivity tensor $\hat{\varepsilon}_e$ were found in the case $\omega\tau \gg 1$ [see Eqs. (20) and (23)]. A new
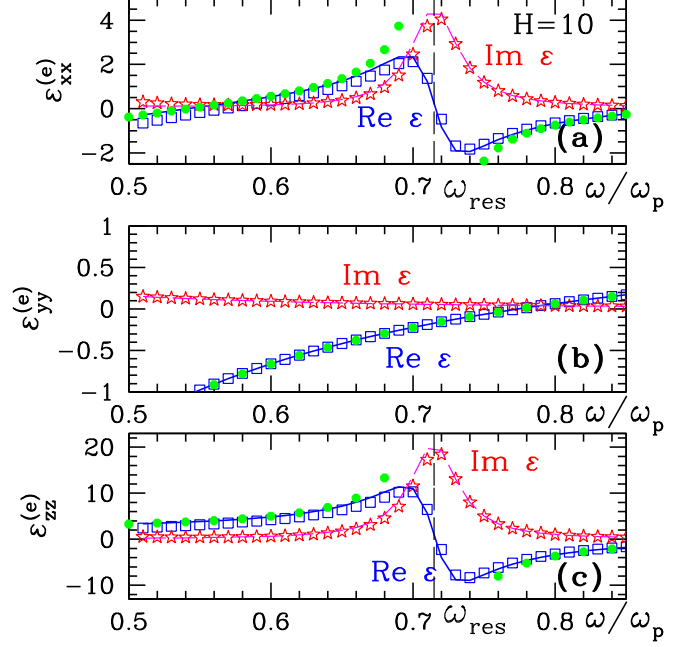

FIG. 7. The same parameters as in Fig. 6 except for $H = 10$. The resonance frequency (shown by the vertical dashed line) shifts to the value $\tilde{\omega}_{res} = \sqrt{p_I/\epsilon + \tilde{H}^2} = 0.72$ [see Eq. (17)]. The green dotted lines show asymptotic results (23).

surface-plasma-like resonance is found for layered structures, with a frequency that depends on the layer thicknesses and the applied dimensionless magnetic field H [see Eq. (17)]. We verified all the analytical results using our numerical scheme for calculating the properties of composites with a periodic microstructure [6,7,10–12,14,15]. Different unit cells of the periodic composite are shown in the top part of Figs. 2, 5, 10, and 12. The number of Fourier components in 3D calculations was between 20 and 28 in each direction and up to 90 in 2D calculations.

In Fig. 2 we show the diagonal components of the macroscopic electric permittivity tensor $\hat{\varepsilon}_e$ versus dimensionless frequency $\tilde{\omega}$ for a structure with $p_M = 0.6$ and $p_I = 1 - p_M = 0.4$ in the case when $H = 0$. Analytical results from Eq. (8) (shown by lines) and numerical results (shown by open symbols) are in good agreement. The zz component of the permittivity tensors demonstrates a strong resonance, at a frequency that depends on the slab thickness, while in the xx and yy component of $\hat{\varepsilon}_e$ there is no resonance [all in accordance with Eqs. (8), (20), and (23)]. A vertical dashed line in Fig. 2(c) shows the resonance frequency value $\omega_{res} = 0.63\omega_p$ for $p_I = 0.4$, $\varepsilon_0 = \varepsilon_I = 0$ [see Eq. (17)]. In Figs. 2(a) and 2(b), a vertical dashed line shows the frequency $\tilde{\omega} = \sqrt{p_M/\bar{\varepsilon}} = 0.78$ [in accordance with Eq. (21)] when $\varepsilon_{xx}^{(e)} = \varepsilon_{yy}^{(e)} = 0$. The asymptotic solutions from Eqs. (21) and (22) are shown by a green dotted line and are again in good agreement with numerical results.

Similar drawings are shown in Fig. 3 for other values of ε_I and p_I. The resonance frequency in the $\varepsilon_{zz}^{(e)}$-tensor component shifts from $\tilde{\omega}_{res} = \sqrt{p_I/\epsilon} = 0.63$ (for $\varepsilon_i = 1$ and $p_I = 0.4$ in Fig. 2) to $\tilde{\omega}_{res} = \sqrt{p_I/\epsilon} = 0.43$ (for $\varepsilon_I = 3$ and $p_I = 0.4$ in Fig. 3), in full agreement with Eq. (17). The

FIG. 9. Resonance frequency $\tilde{\omega}_{res}$ given by Eq. (17) vs applied magnetic field H for different volume fractions of dielectric slabs p_I: 0.2 and 0.7 (with $\varepsilon_I = 1$), 0.4 (with $\varepsilon_I = 2$), and 0.8 (with $\varepsilon_I = 3$), respectively. $\tilde{\tau} = 30$, $\varepsilon_0 = 1$.
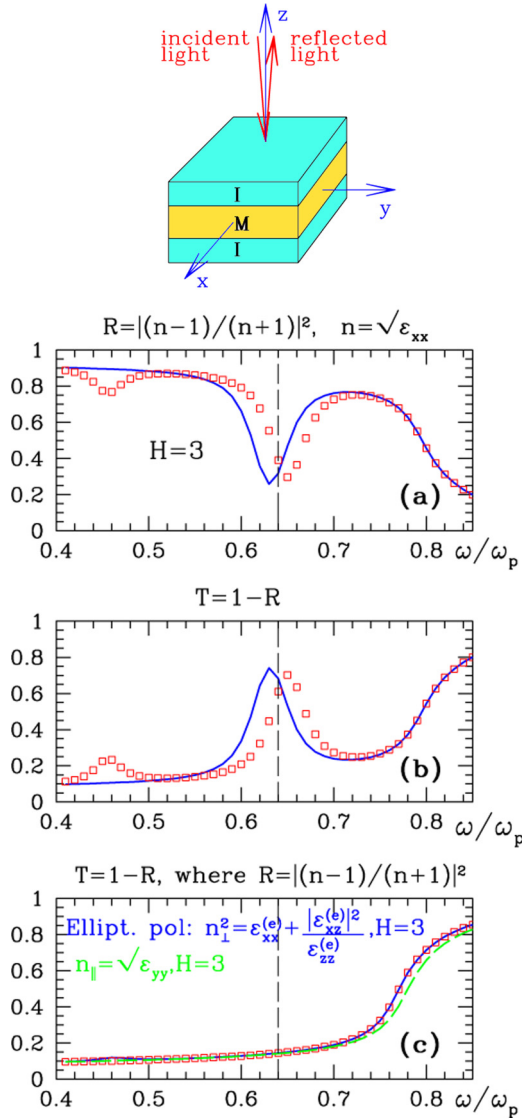

FIG. 8. (a), (b) Calculated reflectance $R = |(n_x - 1)/(n_x + 1)|^2$ (a) and transmittance $T = 1 - R$ (b) coefficients spectra. Here it was assumed that the light is linearly polarized along the x-axis, with $n_x = \sqrt{\varepsilon_{xx}^{(e)}}$ taken from Fig. 6, while $\tilde{\tau} = 30$, $p_M = 0.6$, $p_I = 0.4$, and $H = 3$. (c) Real transmittance $T = 1 - R$ for elliptically polarized light beam with $n_\perp$ given by Eq. (25). The well-pronounced resonance shown in (a), (b) does not lead to ELT. This is reminiscent of the behavior of $\varepsilon_{yy}^{(e)}$, which does not exhibit a resonance, and therefore there is also no ELT when the light is polarized along y. The green dashed curve shows the transmittance for light polarized along the $y \parallel \mathbf{B}$ axis with $n_y = \sqrt{\varepsilon_{yy}^{(e)}}$. Analytical results are shown by the solid lines, while the numerical results are shown by open squares.

reflectance $R = |(n - 1)/(n + 1)|^2$ (where $n = \sqrt{\varepsilon_{xx}^{(e)}}$) and the transmittance $T = 1 - R$ are shown in Fig. 4 versus $\tilde{\omega}$ for the case of light propagating along the z-axis. The transparency window near the resonance frequency $\omega_{res} = 0.63\omega_p$ is well-pronounced.

Figures 5–7 show that the application of an external static magnetic field changes the resonances drastically: The resonance in the $\varepsilon_{xx}^{(e)}$ component is now permitted in full agreement
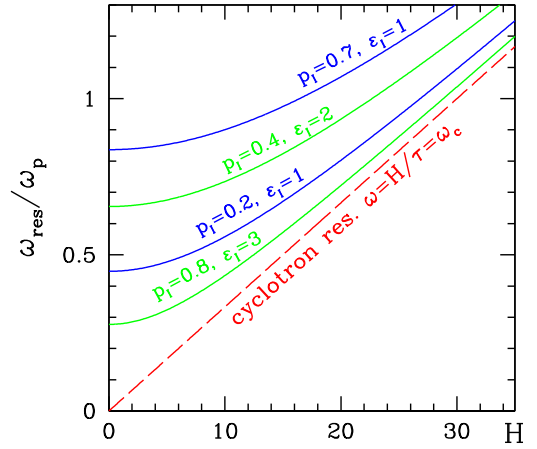
with Eqs. (20) and (23), and its value is given by $\omega_{res} = \omega_p\sqrt{p_I/\epsilon + \tilde{H}^2}$ [see Eq. (17)]. Figures 5, 6, and Eq. (23) show that the Hall component $\varepsilon_H^{(e)}$ also has a resonance. By contrast, the $\varepsilon_{yy}^{(e)}$ component has no resonance. The hypothetical reflectance and transmittance spectra (when $n_x = \sqrt{\varepsilon_{xx}^{(e)}}$) for this are shown in Figs. 8(a) and 8(b). The ELT would be observed in this case, but in the presence of a magnetic field the light will be elliptically polarized, and $n_\perp$ [given by Eq. (25)] instead of n_x should be used in the analytical expressions for R and T. As a result, there is no ELT in this case [see Fig. 8(c), Eq. (25), and the text right after it]. The transmittance coefficient T is also shown for the case of parallel slabs with holes and grooves with and without a magnetic field in Figs. 10(c), 11(c), and 12(c). The values of the LSP resonance frequencies are shown versus H in Fig. 9 and they are in agreement with Eq. (17).

As mentioned above, the resonance in the xx-component can be allowed also by spoiling the symmetry of the microstructure. Thus, the presence of cylindrical holes in a metal layer makes the SP resonance (see resonance no. 2 in Fig. 10) appear near the frequency $\tilde{\omega}_{res} = \sqrt{p_I/\epsilon} = 0.45$, as predicted by Eq. (17) for $H = 0$. A second resonance [see resonance no. 1 in Fig. 10] then appears at a frequency near $\tilde{\omega}_{res} = \sqrt{1/2} = 0.71$ [see Eq. (29)] and is associated with the LSP localized around the circular hole. A similar drawing is shown in Fig. 11 for other parameters. A similar effect can be achieved if instead of cylindrical holes parallel grooves are made on the top and bottom of the metallic slabs as shown in Fig. 12.

Figure 13 is similar to Fig. 10 but for the radius r of the cylindrical hole in the center of the unit cell (see the top part of Fig. 10) equal to 0.2a (where a is the size of the unit cell). Two resonances appear due to this perturbation: Resonance no. 1 due to LSP [i.e., the surface plasmon localized around the cylindrical hole with a resonance frequency determined by Eq. (28)] and resonance no. 2 near the frequency determined by Eq. (17). This resonance is forbidden at $H = 0$ but is allowed in the presence of cylindrical holes. Green dashed
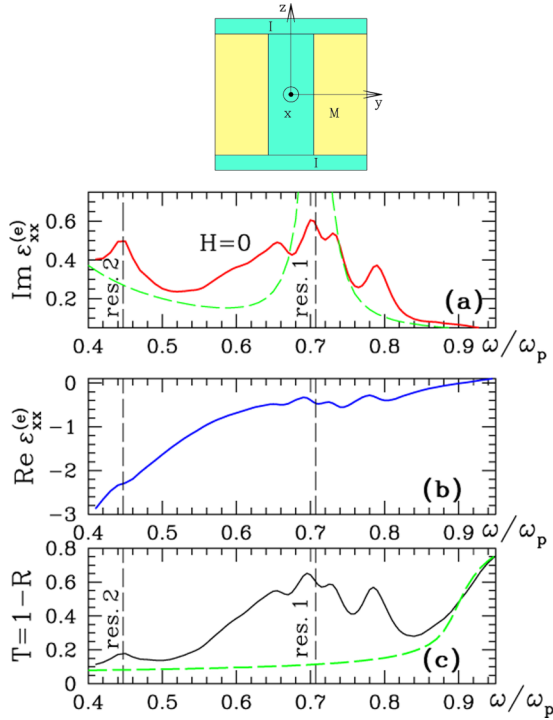
FIG. 10. (a), (b) Imaginary (a) and real (b) parts of the xx-component of the macroscopic permittivity tensor $\hat{\varepsilon}_e$ of an assembly of parallel flat slabs with a cylindrical hole of radius $r = 0.15a$ (where a is the size of the unit cell) at the center of the unit cell (see the top part). There is no applied magnetic field ($H = 0$). Two resonances appear due to the cylindrical hole: Resonance no. 1 due to LPR (i.e., plasmon localized around a circular cylindrical hole) in the middle of the unit cell at $\tilde{\omega}_{res} = \sqrt{1/2} = 0.71$ [see Eq. (29) at $n_x = 1/2$], and resonance no. 2 near the value $\tilde{\omega}_{res} = \sqrt{p_I/\epsilon} = 0.45$, which is determined by Eq. (17). The latter resonance should be forbidden in the absence of a magnetic field but is stimulated by the presence of a cylindrical hole. The green dashed line is obtained by the dilute approximation (DA) using Eq. (28). The resonance frequency obtained by the latter approximation agrees with numerical results, but the amplitude does not. (c) Transmittance $T = 1 - R$ for an elliptically polarized light beam with $n_x = \sqrt{\varepsilon_{xx}^{(e)}}$ and $\varepsilon_{xx}^{(e)}$ taken from (a) and (b). Green dashed curve represents, for comparison, the analytical result obtained for a system of parallel slabs without holes. $\tilde{\tau} = 30$, $p_M = 0.8$, $p_I = 0.2$, $H = 0$, $\varepsilon_0 = \varepsilon_I = 1$. Top: Unit cell used for numerical calculations of MD parallel flat-slab nanostructure, similar to Fig. 2 but with a cylindrical hole at the center of the metallic slab.

lines show the result obtained by reduction of 3D calculations into 2D ones, described in Sec. II E. A red dashed line shows results of a calculation using the dilute approximation [see Eqs. (28) and (29)], while a blue dashed line shows results from using the CM approximation [see Eqs. (30) and (31)]. The resonance frequencies obtained by DA and CM approximations are in agreement with numerical results, while their amplitudes are not.

In Figs. 14(a) and 14(b), we show the xx-component of the macroscopic permittivity tensor $\hat{\varepsilon}_e$ of an assembly of parallel flat slabs with cylindrical holes versus $\tilde{\omega}$ for different values
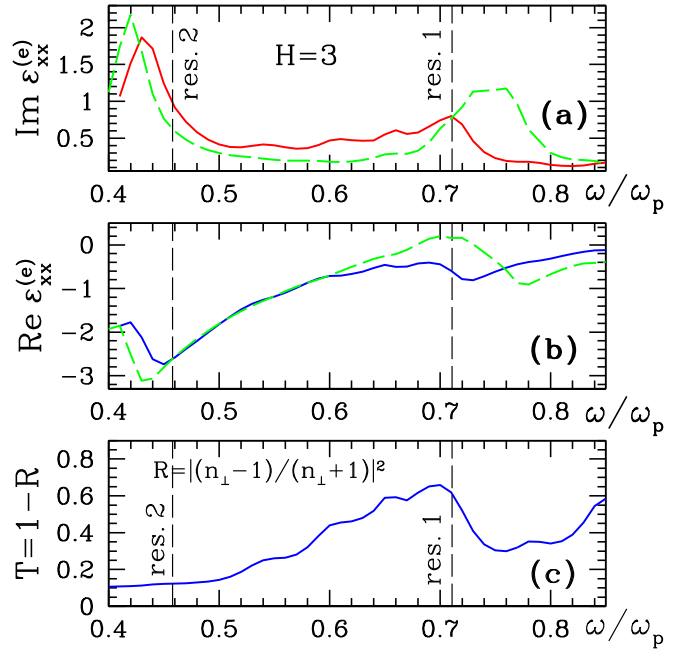

FIG. 11. (a), (b) Similar to Fig. 10 but for a nonzero magnetic field $H = 3$ applied along the y-axis (see the top of Fig. 10). Two resonances appear: Resonance no. 1 due to LSP (localized around the cylinder) at $\tilde{\omega}_{res}(H) = \sqrt{(1 + \tilde{H}^2)/2} = 0.71$ [see Eq. (30)] and resonance no. 2 at $\tilde{\omega}_{res}(H) = \sqrt{p_I/\epsilon + \tilde{H}^2} = 0.46$ [see Eq. (17)]. Green dashed lines show the results obtained when the 3D calculations are reduced to 2D calculations, as described in Sec. II E. $\tilde{\tau} = 30$, $p_M = 0.8$, $p_I = 0.2$, $\varepsilon_{0M} = 1$, $\varepsilon_I = 1$. (c) Transmittance $T = 1 - R$ for an elliptically polarized light beam with $n_\perp$ given by Eq. (25). The well-pronounced resonance no. 2 shown in (a) and (b) does not lead to ELT phenomena.

of the applied magnetic field H. Results were calculated using the dilute approximation [see Eq. (28)]. In Fig. 14(c) we show the resonance frequency $\tilde{\omega}_{res}$ versus the applied magnetic field H. Open squares are the maxima values of Im $\varepsilon_{xx}^{(e)}$ taken from Fig. 14(a), while the dashed red line shows the result of Eq. (29) and the dashed green line shows the result of Eq. (30).

IV. DISCUSSION AND SUMMARY

In summary, a general expression for the resonance frequency of SPs in a metal-dielectric assembly of parallel flat layers or slabs in the presence of an in-plane static magnetic field **B** is found. This resonance depends on **B** and on the slabs' relative thicknesses and permittivities. It has completely different properties and behaviors in comparison with the LSP resonance. To observe it in the xx component of the permittivity tensor, one needs to apply a magnetic field or make microstructural heterogeneities such as holes or grooves. However, in many cases this does not lead to ELT phenomena, in contrast with the LSP resonance, which was shown analytically to appear when a magnetic field is applied. This resonance is absent in the yy tensor component of the permittivity tensor $\hat{\varepsilon}_e$, again in contrast with the LSP
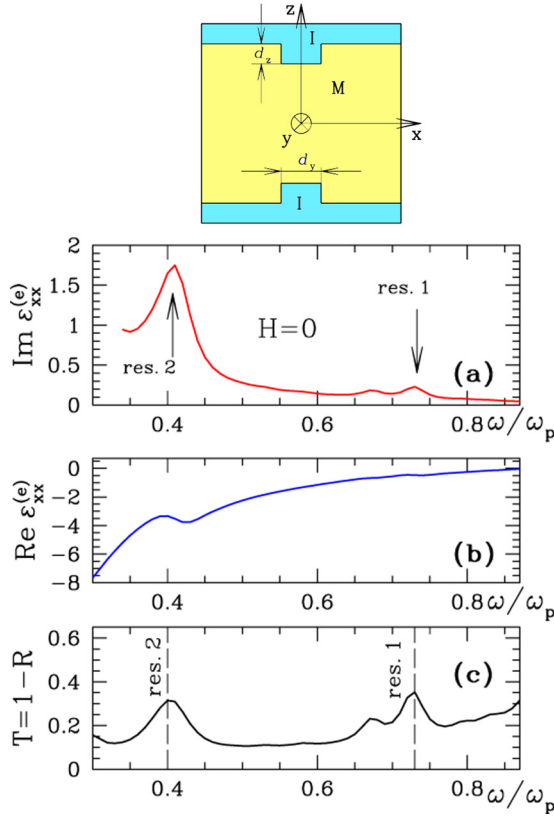
FIG. 12. (a), (b) The same as Fig. 10 but with grooves as shown in the top part of this figure. Resonance no. 1 at $\tilde{\omega} \simeq 0.73$ is due to a surface plasmon localized near the groove (when that groove is bar-shaped with a square cross-section, the exact resonance frequency is unknown). Resonance no. 2 appears near $\tilde{\omega}_{\mathrm{res}} \simeq 0.4$, which is close to $\tilde{\omega}_{\mathrm{res}} = \sqrt{p_I/\epsilon} = 0.45$, the value at which there should not be a resonance in the absence of a magnetic field. Here that resonance is stimulated by the presence of grooves. (c) Transmittance $T = 1 - R$ for an elliptically polarized light beam with $n_x = \sqrt{\varepsilon_{xx}^{(e)}}$ and $\varepsilon_{xx}^{(e)}$ taken from (a) and (b). Top: Unit cell used for numerical calculations of MD parallel slab nanostructure with grooves of sizes $d_y = a$, $d_x = 0.2a$, $d_z = 0.1a$. Upper and lower "I"-slabs are dielectric with $\varepsilon_I = 1$ and $p_I = 0.2$, while "M"-slab is a conductor with $\hat{\varepsilon}_M$ given by Eq. (2) with $\varepsilon_0 = 1$ and $p_M = 0.8$. $\tilde{\tau} = 30$.

resonance, which is present in both the *xx* and *yy* tensor components.

Asymptotically exact (in limit $\omega\tau \gg 1$) analytical expressions were derived for the macroscopic permittivity tensor $\hat{\varepsilon}_e$ and for the frequency of a new surface plasmonic-like resonance. In the absence of the magnetic field, this resonance appears only in the *zz* component of the macroscopic permittivity tensor $\hat{\varepsilon}_e$, i.e., only when light is propagating parallel to the slab surfaces and its electric field is perpendicular to these surfaces. However, the application of an in-plane magnetic field induces this resonance even in the *xx* tensor component (i.e., when light is propagating perpendicular to the slab surfaces with a polarization perpendicular to the applied magnetic field). The resonance is induced also in the off-diagonal Hall tensor component. Even in the presence of a magnetic field, the resonance is absent in the *yy* tensor component. We showed numerically that the spoiling of the
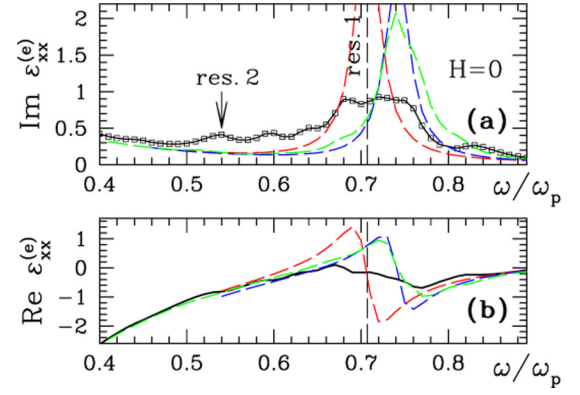

FIG. 13. Similar to Fig. 10 except for the radius $r = 0.2a$ (where a is the size of the unit cell) of the cylindrical hole in the center of the unit cell (see the top part of Fig. 10). There is no applied magnetic field ($H = 0$). Two resonances appear due to the cylindrical hole at the center of the unit cell: Resonance no. 1 due to LSP (i.e., the surface plasmon localized around the cylindrical hole) at $\omega_{\mathrm{res}}/\omega_p = \sqrt{1/2} = 0.71$ shown by a vertical dashed line—see Eqs. (28) and (29)—and resonance no. 2 near the frequency determined by Eq. (17) and forbidden when $H = 0$ but stimulated by the presence of cylindrical holes. Green dashed lines show the numerical result obtained when the 3D computations are reduced to 2D ones, as described in Sec. II E. The red dashed line shows the results of a calculation using the dilute approximation of Eqs. (28) and (29) while the blue dashed line shows results obtained using the CM approximations [see Eqs. (30) and (31)]. The resonance frequencies obtained by DA and CM approximations are in agreement with numerical results, while the amplitudes are not. $\tilde{\tau} = 30$, $p_M = 0.8$, $p_I = 0.2$, $\varepsilon_0 = 1$, $\varepsilon_I = 1$.

high symmetry of the slab surfaces, e.g., by making holes or grooves in the metallic slabs, also induces the resonance in the *xx* tensor component.

All our analytical results agree qualitatively and even quantitatively with the results of numerical calculations on periodic nanostructures performed using the numerical scheme of Refs. [6,7,10,11,17]. Our method of calculation assumes that the hole sizes and the lattice constant of the hole lattice are small compared to the wavelength of light. We emphasize that in our calculations we have not used any absolute values, but only relative ones—namely, the ratio between the slab thicknesses and the ratio between hole sizes and the distance between the holes. Even though we have used the quasistatic approximation, we believe that the effects predicted here will persist even for lattice constants comparable to the wavelength.

The phenomena discussed here can be used for manipulating the transmission of light through a sandwichlike metal-dielectric assembly of parallel layers by applying an external magnetic field. This possibility arises whenever the Hall resistivity of the metal layers exceeds their Ohmic resistivity.

The phenomena discussed in this paper depend on the dimensionless magnetic field $H = \omega_c \tau = \mu|\mathbf{B}|$. Bismuth [36,74] is a metal where H can easily reach large enough values with easily achievable magnetic fields. That is because the low carrier density ($\sim 3 \times 10^{17}$ cm^3) can make the carrier cyclotron frequency ω_c equal to or greater than the bulk plasma frequency ω_p. Another possibility is to use films of
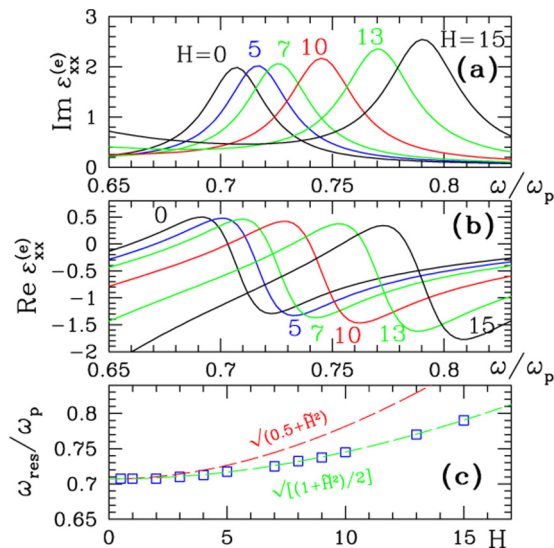
FIG. 14. Imaginary (a) and real (b) parts of the xx-component of the macroscopic permittivity tensor $\hat{\varepsilon}_e$ of an assembly of parallel flat slabs with cylindrical holes of radius $r = 0.15a$ (where a is the size of the unit cell) (see the top part of Fig. 10) vs $\tilde{\omega}$ for different values of the applied magnetic field H. The results are obtained using the dilute approximation [see Eq. (28)]. When $H = 0$, the LSP resonance appears at $\tilde{\omega}_{\rm res} = \sqrt{1/2} = 0.71$, which increases with H according to Eq. (30). (c) The resonance frequency $\tilde{\omega}_{\rm res}$ vs the applied magnetic field H. Open squares are the maxima values of Im $\varepsilon_{xx}^{(e)}$ taken from (a), while the dashed red line is the result of Eq. (29) and the dashed green line is the result of Eq. (30). $\tilde{\tau} = 30$, $p_M = 0.8$, $p_I = 0.2$, $H = 0$, $\varepsilon_0 = 1$, $\varepsilon_I = 1$.

highly doped semiconductors such as GaAs [35] and InAs. The value of $\omega_p \tau$ in this case can be of the same order of magnitude as in conventional metals—in our calculations we assumed $\omega_p \tau = 30$, while for a typical free-electron metal like Al we have $\omega_p \tau \simeq 100$. Thus such anisotropic, magnetic-field-dependent, extraordinary optical transmission in the infrared range of frequencies can be sought in heavily doped semiconductor films with an array of holes with a submicron periodicity. In transition-metal films of Ag or Au, where surface plasmons are easily observed in visible light, stronger magnetic fields would be needed in order to observe the behavior described here. The detailed treatment would also require going beyond the quasistatic approximation.

We have used the Drude approximation (2) for the local permittivity tensor since it allows us to perform analytical evaluations and to predict the optical behavior and features of the sandwichlike slab system under consideration. For the case of real experiment, it is possible to take not the Drude approximation but measured values of the local permittivity tensor. Then the effective permittivity tensor as well as the other optical properties can be found numerically using Eqs. (7) and (8) and other relations presented in this manuscript. The obtained optical features should be at least qualitatively similar to those obtained above.

It would be interesting to perform experiments on homogeneous and/or perforated metal-dielectric flat slabs nanostructures, for which we have now presented exact theoretical predictions.

[1] T. W. Ebbesen, H. J. Lezec, H. F. Ghaemi, T. Thio, and P. A. Wolff, Extraordinary optical transmission through subwavelength hole arrays, Nature (London) **391**, 667 (1998).

[2] H. A. Bethe, Theory of diffraction by small holes, Phys. Rev. **66**, 163 (1944).

[3] A. Roberts, Electromagnetic theory of diffraction by a circular aperture in a thick, perfectly conducting screen, J. Opt. Soc. Am. A **4**, 1970 (1987).

[4] *Electromagnetic Theory of Gratings*, edited by R. Petit (Springer-Verlag, Berlin, 1980).

[5] H. Raether, *Surface Plasmons* (Springer-Verlag, Berlin, 1988).

[6] D. J. Bergman and Y. M. Strelniker, Anisotropic ac Electrical Permittivity of a Periodic Metal-Dielectric Composite Film in a Strong Magnetic Field, Phys. Rev. Lett. **80**, 857 (1998).

[7] Y. M. Strelniker and D. J. Bergman, Optical transmission through metal films with a subwavelength hole array in the presence of a magnetic field, Phys. Rev. B **59**, R12763(R) (1999).

[8] Y. M. Strelniker, Theory of optical transmission through elliptical nanohole arrays, Phys. Rev. B **76**, 085409 (2007).

[9] Y. M. Strelniker and D. J. Bergman, Magneto-optical properties of metal-dielectric composites with a periodic microstructure, Eur. Phys. J. Appl. Phys. **7**, 19 (1999).

[10] D. J. Bergman and Y. M. Strelniker, Calculation of strong-field magneto-transport in some periodic composites, Phys. Rev. B **49**, 16256 (1994).

[11] Y. M. Strelniker and D. J. Bergman, Theory of magneto-transport in a composite medium with periodic microstructure for arbitrary magnetic fields, Phys. Rev. B **50**, 14001 (1994).

[12] Y. M. Strelniker and D. J. Bergman, Interference of current distortion patterns and magnetoresistance anisotropy in a composite with periodic microstructure, Phys. Rev. B **53**, 11051 (1996).

[13] D. J. Bergman and Y. M. Strelniker, Duality Transformation in a Three-Dimensional Conducting Medium with Two-Dimensional Heterogeneity and an In-Plane Magnetic Field, Phys. Rev. Lett. **80**, 3356 (1998).

[14] D. J. Bergman and Y. M. Strelniker, Strong-field magneto-transport in a two-constituent columnar composite medium where the constituents have comparable resistivity tensors, Phys. Rev. B **86**, 024414 (2012).

[15] D. J. Bergman and Y. M. Strelniker, Magneto-transport in conducting composite films with a disordered columnar microstructure and an in-plane magnetic field, Phys. Rev. B **60**, 13016 (1999).

[16] A. K. Sarychev, D. J. Bergman, and Y. M. Strelniker, High field magneto-transport in a percolating medium, Europhys. Lett. **21**, 851 (1993).

[17] Y. M. Strelniker and D. J. Bergman, Transmittance and transparency of subwavelength-perforated conducting films in the presence of a magnetic field, Phys. Rev. B **77**, 205113 (2008).

[18] Y. M. Strelniker and D. J. Bergman, Strong angular magneto-induced anisotropy of Voigt effect in metal-dielectric metamaterials with periodic nanostructures, Phys. Rev. B **89**, 125312 (2014).

[19] Y. M. Strelniker and D. J. Bergman, Magneto-optical response of a periodic metallic nano-structure, in *Plasmonics: Metallic Nanostructures and Their Optical Properties XIII*, edited by A. D. Boardman and D. P. Tsai, Proceedings of SPIE Vol. 9547 (SPIE, Bellingham, WA, 2015), p. 954705.

[20] T. A. Dorschner and R. J. Vernon, The Voigt-type magneto-Kerr effect in cubic semiconductors having ellipsoidal constant energy surfaces, J. Phys. Chem. Solids **37**, 935 (1976).

[21] D. G. Baranov, A. P. Vinogradov, A. A. Lisyansky, Y. M. Strelniker, and D. J. Bergman, Magneto-optical spaser, Opt. Lett. **38**, 2002 (2013).

[22] G. A. Wurtz, W. Hendren, R. Pollard, R. Atkinson, L. Le Guyader, A. Kirilyuk, Th. Rasing, I. I. Smolyaninov, and A. V. Zayats, Controlling optical transmission through magneto-plasmonic crystals with an external magnetic field, New J. Phys. **10**, 105012 (2008).

[23] V. I. Belotelov, L. L. Doskolovich, and A. K. Zvezdin, Extraordinary Magneto-Optical Effects and Transmission through Metal-Dielectric Plasmonic Systems, Phys. Rev. Lett. **98**, 077401 (2007).

[24] A. B. Khanikaev, A. V. Baryshev, A. A. Fedyanin, A. B. Granovsky, and M. Inoue, Anomalous Faraday effect of a system with extraordinary optical transmittance, Opt. Express **15**, 6612 (2007).

[25] N. Ou, J. H. Shyu, J. C. Wu, and T. H. Wu, Extraordinary optical transmission through dielectric hole-array coated with TbFeCo thin film, IEEE Trans. Magn. **45**, 4027 (2009).

[26] G. Düchs, G. L. J. A. Rikken, T. Grenet, and P. Wyder, Magnetotransverse Scattering of Surface Plasmon Polaritons, Phys. Rev. Lett. **87**, 127402 (2001).

[27] L. E. Helseth, Tunable plasma response of a metal/ferromagnetic composite material, Phys. Rev. B **72**, 033409 (2005).

[28] M. Diwekar, V. Kamaev, J. Shi, and Z. V. Vardeny, Optical and magneto-optical studies of two-dimensional metallodielectric photonic crystals on cobalt films, Appl. Phys. Lett. **84**, 3112 (2004).

[29] B. Sepulveda, L. M. Lechuga, and G. Armelles, Magnetooptic effects in surface-plasmon-polaritons slab waveguides, J. Lightwave Technol. **24**, 945 (2006).

[30] I. S. Maksymov, Magneto-plasmonics and resonant interaction of light with dynamic magnetisation in metallic and all-magneto-dielectric nanostructures, Nanomaterials **5**, 577 (2015).

[31] B. Hu, B. Y. Gu, Y. Zhang, and M. Liu, Transmission interference tuned by an external static magnetic field in a two-slit structure, Appl. Phys. Lett. **95**, 121103 (2009).

[32] G. Dresselhaus, A. F. Kip, and C. Kittel, Plasma resonance in crystals: Observations and theory, Phys. Rev. **100**, 618 (1955).

[33] Y. M. Strelniker and D. J. Bergman, Thermoelectric response of a periodic composite medium in the presence of a magnetic field: Angular anisotropy, Phys. Rev. B **96**, 235308 (2017).

[34] Y. M. Strelniker and D. J. Bergman, Angular anisotropy of thermoelectric properties of a periodic composite medium in the presence of a magnetic field, J. Electron. Mater. **48**, 4507 (2019).

[35] M. Tornow, D. Weiss, K. von Klitzing, K. Eberl, D. J. Bergman, and Y. M. Strelniker, Anisotropic Magnetoresistance of a Classical Antidot Array, Phys. Rev. Lett. **77**, 147 (1996).

[36] G. J. Strijkers, F. Y. Yang, D. H. Reich, C. L. Chien, P. C. Searson, Y. M. Strelniker, and D. J. Bergman, Magnetoresistance anisotropy of a Bi antidot array, IEEE T. Magm. **37**, 2067 (2001).

[37] K. D. Fisher and D. Stroud, Conductivity and magnetoresistance of a periodic composite by network discretization, Phys. Rev. B **56**, 14366 (1997).

[38] H. F. Ghaemi, T. Thio, D. E. Grupp, T. W. Ebbesen, and H. J. Lezec, Surface plasmons enhance optical transmission through subwavelength holes, Phys. Rev. B **58**, 6779 (1998).

[39] L. Martin-Moreno, F. J. Garcia-Vidal, H. J. Lezec, K. M. Pellerin, T. Thio, J. B. Pendry, and T. W. Ebbesen, Theory of Extraordinary Optical Transmission through Subwavelength Hole Arrays, Phys. Rev. Lett. **86**, 1114 (2001).

[40] W. L. Barnes, A. Dereux, and T. W. Ebbesen, Surface plasmon subwavelength optics, Nature (London) **424**, 824 (2003).

[41] A. Polman and H. A. Atwater, Plasmonics: Optics at the nanoscale, Mater. Today **8**, 56 (2005).

[42] *Modern Plasmonics*, edited by A. A. Maradudin, J. R. Sambles, and W. L. Barnes (Elsevier, Amsterdam, 2014), pp. 1–23.

[43] F. J. G. I. de Abajo, Light transmission through a single cylindrical hole in a metallic film, Opt. Express **10**, 1475 (2002).

[44] X. Lu, H. L. Shi, and Y. Y. Lu, Vertical mode expansion method for transmission of light through a single circular hole in a slab, J. Opt. Soc. Am. A **31**, 293 (2014).

[45] Y.-Q. Lu, X.-Y. Cheng, M. Xu, J. Xu, and J. Wang, Extraordinary transmission of light enhanced by exciting hybrid states of Tamm and surface plasmon polaritons in a single nano-slit, Acta Phys. Sin.-Chin. Ed.-ER **65**, 204207 (2016).

[46] Z.-Q. Gong and J.-Q. Liu, Role of localised surface plasmon polaritons coupling in optical transmission through double-layer metal apertures, Chin. Phys. B **19**, 1674 (2010).

[47] Z. B. Li, W. Y. Zhou, W. G. Yan, and J. G. Tian, Near-field enhancement through a single subwavelength aperture with gaps inside, Plasmonics **6**, 149 (2011).

[48] A. Degiron and T. W. Ebbesen, The role of localized surface plasmon modes in the enhanced transmission of periodic subwavelength apertures, J. Opt. A-Pure Appl. Opt. **7**, S90 (2005).

[49] D. He, T. Y. Zhang, L. Liu, S. X. Guo, and Z. J. Liu, Refractive index sensing of monolayer molecules using both local and propagating surface plasmons in mid-infrared metagrating, Appl. Sci. **9**, 1524 (2019).

[50] R. Gordon, A. G. Brolo, A. McKinnon, A. Rajora, B. Leathem, and K. L. Kavanagh, Strong Polarization in the Optical Transmission through Elliptical Nanohole Arrays, Phys. Rev. Lett. **92**, 037401 (2004).

[51] K. J. K. Koerkamp, S. Enoch, F. B. Segerink, N. F. van Hulst, and L. Kuipers, Strong Influence of Hole Shape on Extraordinary Transmission through Periodic Arrays of Subwavelength Holes, Phys. Rev. Lett. **92**, 183901 (2004).

[52] Y. Fleger, M. Rosenbluh, Y. M. Strelniker, D. J. Bergman, and A. N. Lagarkov, Controlling the optical spectra of gold nano-islands by changing the aspect ratio and the inter-island distance: theory and experiment, Eur. Phys. J. B **81**, 85 (2011).

[53] J. Müller, C. Sönnichsen, H. von Poschinger, G. von Plessen, T. A. Klar, and J. Feldmann, Electrically controlled light scattering with single metal nanoparticles, Appl. Phys. Lett. **81**, 171 (2002).

[54] J. B. Keller, A theorem on the conductivity of a composite medium, J. Math. Phys. **5**, 548 (1964).

[55] A. M. Dykhne, Conductivity of a two-dimensional two-phase system, Zh. Eksp. Teor. Fiz. **59**, 110 (1970) [Sov. Phys. JETP **32**, 63 (1971)]; Anomalous resistance of a plasma in a strong magnetic field, Zh. Eskp. Teor. Fiz. **59**, 641 (1970) [Sov. Phys. JETP **32**, 348 (1971)].

[56] Y. M. Strelniker and D. J. Bergman, Exact relations between macroscopic moduli of composite media in three-dimensions: Application to magnetoconductivity and magneto-optics of 3D composites with related columnar microstructures, Phys. Rev. B **67**, 184416 (2003).

[57] M. Babinet, Memoires d'optique méteorologique, Acad. Sci. Paris C. R. **4**, 638 (1837).

[58] D. J. Bergman and Y. M. Strelniker, Macroscopic magnetoresistance of an assembly of parallel flat conducting slabs, Phys. Rev. B **100**, 214204 (2019).

[59] A. Hamzah, Multilayer-tuned surface plasmon modes using molecular nanolayer of (3-mercaptopropyl)trimethoxysilane applicable for nanobiosensing application, Mater. Design **155**, 99 (2018).

[60] B. Liu, C. J. Tang, J. Chen, N. Y. Xie, L. Zheng, and S. Wang, Tri-band absorption enhancement in monolayer graphene in visible spectrum due to multiple plasmon resonances in metal-insulator-metal nanostructure, Appl. Phys. Express **11**, 072201 (2018).

[61] O. Yeshchenko, I. Bondarchuk, S. Malynych, Y. Galabura, G. Chumanov, and I. Luzinov, Surface plasmon modes of sandwich-like metal-dielectric nanostructures, Plasmonics **10**, 655 (2015).

[62] S. X. Zhang, S. Liu, S. F. Yang, C. T. Wang, and X. G. Luo, Near-field Moire effect with dielectric-metal-dielectric sandwich structure, J. Nanophoton. **7**, 073080 (2013).

[63] J. Salvi and D. Barchiesi, Measurement of thicknesses and optical properties of thin films from surface plasmon resonance (SPR), Appl. Phys. A **115**, 245 (2014).

[64] Y. M. Strelniker, D. Stroud, and A. O. Voznesenskaya, Control of extraordinary light transmission through perforated metal films using liquid crystals, Eur. Phys. J. B **52**, 1 (2006).

[65] Y. M. Strelniker, D. Stroud, and A. O. Voznesenskaya, Magneto-optical features and extraordinary light transmission through perforated metal films filled with liquid crystals, J. Appl. Phys. **99**, 08H702 (2006).

[66] D. J. Bergman and D. Stroud, Physical properties of macroscopically inhomogeneous media, Solid State Phys. **46**, 147 (1992).

[67] G. W. Milton, *The Theory of Composites* (Cambridge University Press, Cambridge, 2002).

[68] R. E. De Wames and W. F. Hall, Magnetic-Field Effect on Plasma-Wave Dispersion in a Dielectric Layer, Phys. Rev. Lett. **29**, 172 (1972).

[69] K. L. Kliewer and R. Fuchs, Theory of dynamical properties of dielectric surfaces, in *Advances in Chemical Physics*, edited by I. Prigogine and S. A. Rice (John Wiley & Sons, Hoboken, NJ, 2007), Chap. 4, pp. 355–541.

[70] M. S. Kushwaha and P. Halevi, Magnetoplasmons in thin-films in the Voigt configuration, Phys. Rev. B **36**, 5960 (1987).

[71] M. I. Azbel and E. A. Kaner, The theory of cyclotron resonance in metals, Zh. Eskp. Teor. Fiz. **30**, 811 (1956) [Sov. Phys. JETP **3**, 772 (1956)].

[72] J. B. Pendry, L. Martin-Moreno, and F. J. Garcia-Vidal, Mimicking surface plasmon with structured surfaces, Science **305**, 847 (2004).

[73] D. J. Bergman and D. G. Stroud, High-field magnetotransport in composite conductors: Effective-medium approximation, Phys. Rev. B **62**, 6603 (2000).

[74] R. L. Blewitt and A. J. Sievers, Magnetic-field-induced far-infrared transmission in bismuth, J. Low Temp. Phys. **13**, 617 (1973).